Proceeding of the 2004 American Control Conference
Boston, Massachusetts June 30 - July 2, 2004

Stability Considerations and Performance of Wide Dynamic Range, Ambient Light Active Rejection Circuits in Photodiode Receivers

Al-Thaddeus Avestruz, John I. Rodriguez, Roderick Hinman, Gary Livshin, Elmer C. Lupton
Talking Lights, LLC
1340 Soldiers Field Road
Brighton, MA 02135
e-mail: avestruz@mit.edu

Steven B. Leeb
Massachusetts Institute of Technology
77 Massachusetts Avenue
Cambridge, MA 02139

***Abstract* – We discuss several issues in active circuits for the rejection of ambient photocurrent over a wide dynamic range. These circuits are important for diffuse, free-space optical communications that operate over a variety of indoor and outdoor lighting conditions. In addition, we introduce, analyze and demonstrate a second-order rejection circuit based on a low noise gyrator in tandem with the input transimpedance amplifier. Excellent rejection is achieved over three orders of magnitude in ambient photocurrent. The measured transient performance agrees well with theory and simulations, and the rejection circuit was demonstrated with IrDA signals for outdoor applications in direct sunlight.**

I. INTRODUCTION

There is a steady proliferation of free-space optical communications systems that use diffuse lights sources such as infrared LEDs for IrDA, and modulated non-flickering illumination using visible LEDs and fluorescent lights [1] for marking and beaconing. Indoor and outdoor marking and beaconing combined with context aware computing find applications in guiding and aiding the disabled [2, 3], security [4], obstacle and hazard marking in the military [5], among others.

These optical communications systems require a reliable receiver that can operate under a variety of demanding ambient lighting conditions: ranging from direct sunlight to total darkness, to mixed lighting conditions, and to sources with high power line harmonic content [6]. The demands imposed by ambient lighting are further exacerbated by the typical use of wide angle-of-acceptance detectors [7].

Under extreme conditions, the ratio between ambient light intensity and signal can be over 120 dB. Gas discharge lamps can have large harmonic contents that extend into the kilohertz range. With carrier frequencies on the order of only 100 kHz in modulated fluorescent lights, rejection circuits that achieve good signal separation from the background are required so that proceeding amplifier stages do not saturate. Because these signals are small, the typical front-end stage for a photodiode receiver is a high gain, low-noise transimpedance amplifier, followed by one or more filtering stages.

The requirements for rejection circuits include minimal noise contribution, performance over a wide dynamic range, and stability. The simplest approach is a passive LR or RC first-order high-pass filter. In many cases, a second-order filter response is necessary. Passive LC filters provide a low-noise solution, but suffer from the difficulty of integrating inductors and from the impracticality, even with discretes, of the large values of inductance required for frequencies below a few megahertz. Active rejection circuits usually use feedback to behave like inductors, but proper design must consider closed-loop stability as well as noise performance.

One way to design a high-pass rejection circuit is to incorporate the high gain amplifier in the feedback loop [8]. This usually introduces more in-band noise than a tandem rejection circuit and makes signal gain control more difficult. In both cases, the difficulty with the design of photodiode rejection circuits is that the loop gain changes with the ambient photocurrent, hence changing the closed-loop response and if not mitigated, ultimately affects the rejection performance and loop stability.

We discuss designs for the ambient photocurrent rejection, considerations for stability and compensation, along with associated performance tradeoffs.

II. FRONT-END AMBIENT PHOTOCURRENT REJECTION

Ambient photocurrent rejection circuits generally have a high-pass characteristic. The order of this high-pass response determines the attenuation of DC and other unwanted low frequency interference. Under conditions where ambient interference is large, it is typically advantageous to remove this interference at the front-end gain stage so that maximal gain can be achieved at the signal frequency without saturation. A large front-end gain that contributes minimal noise is especially important if noisier active filter stages follow.

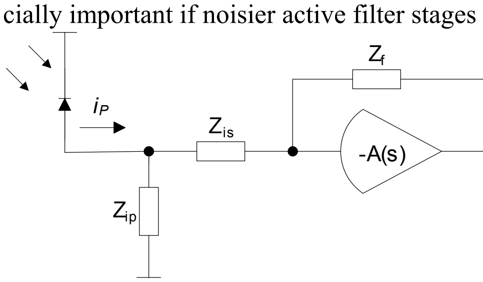

Figure 1: General Impedance Representation of Photoreceiver Front Ends.

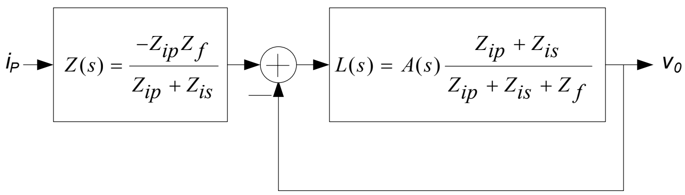

Figure 2: Photoreceiver Unity-Feedback Block Diagram

Figure 1 shows a transimpedance front end in terms of its shunt (Z_{ip}), series (Z_{is}), and feedback (Z_f) impedances. This reduces to a general block diagram of the op amp feedback loop in Figure 2, with the ideal response given by the transimpedance gain $Z(s)$ and the stability determined by the loop transmission $L(s)$. $A(s)$ is the op amp transfer function and is modeled by A_0 / s.

III. PASSIVE REJECTION CIRCUITS

Passive rejection circuits provide us with an analogue with which to base our analysis of active circuits. In the analysis, the photodetector (typically a PIN diode) is modeled as an ideal current source i_P with a parasitic junction capacitance C_p.

A. First-Order Rejection

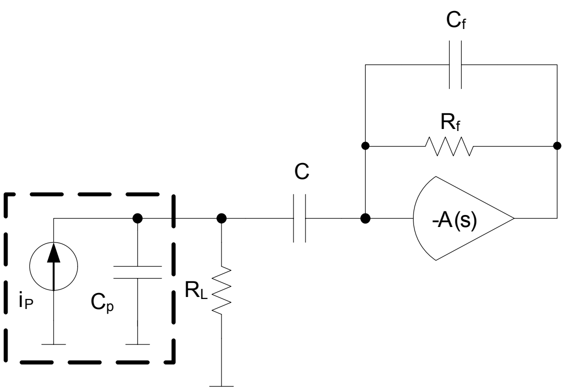

Figure 3: Capacitively Coupled Transimpedance Amplifier

The disadvantage of the capacitively-coupled transimpedance amplifier in Figure 3 is that the voltage drop across R_L at high DC light levels causes the photodiode to saturate. The added noise current density $i_n = \sqrt{4kT/R_L}$ and the gain-bandwidth product of the op-amp ($R_L \gg \left|R_f / A(s)\right|$ at signal frequencies) impose a lower limit on R_L. At moderate transimpedance gains and relatively low ambient light levels, acceptable performance can be achieved.

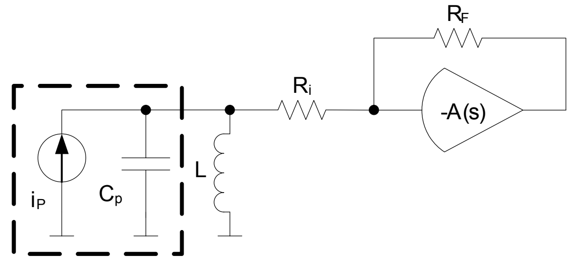

Figure 4: Inductively Shunted Transimpedance Amplifier

The advantage of an inductively shunted transimpedance amplifier is that the maximum available DC voltage is impressed on the photodiode at ambient light levels. Because the junction capacitance C_p decreases as the reverse-bias voltage of the photodiode increases, the inductively shunted amplifier helps to increase bandwidth. Proper choice of the L/R_i time constant prevents both the saturation of both the photodetector and the transimpedance amplifier.

The transimpedance gain with an ideal op amp and $C_p = 0$ is given by

$$Z(s) = -R_F \frac{\tau s}{1+\tau s} \tag{1}$$

where $\tau = R_L C$ for capacitively coupled and $\tau = L / R_i$ for inductively shunted amplifiers.

The stability of the first-order circuits $C_p = 0$ is determined by their loop transmissions:

$$L(s) = A(s) \frac{1+\tau s}{1+\tau' s} \tag{2}$$

for the capacitively coupled amplifier with $\tau' = (R_L + R_F)C$;

$$L(s) = A(s) \frac{R_i}{R_i + R_F} \frac{1+\tau s}{1+\tau' s} \tag{3}$$

for the inductively shunted amplifier with $\tau' = L/(R_i + R_F)$.

Non-zero C_p makes the loop transmission second order and may cause instability. In the capacitively coupled amplifier, if $C_p \ll C$ a pole is introduced at $\tau \approx (R_L \parallel R_f)C_p$. A lead zero via C_f is the usual compensation strategy [9].

In the inductively shunted amplifier, C_p resonates with L. For large values of R_i, this pole pair is under-damped. The loop transmission is given by

$$L(s) = A(s) \frac{R_i}{R_i + R_f} \frac{s^2 + 2\zeta\omega_p + \omega_p{}^2}{s^2 + 2\zeta'\omega_p + \omega_p{}^2}, \tag{4}$$

where $\omega_p = 1\big/\sqrt{LC_p}$, $\zeta = \sqrt{L/C_p}\,/\,2R_i$, and $\zeta' = \sqrt{L/C_p}\,/\,2(R_i + R_F)$.

B. *Second-Order Rejection*

As lighting conditions become more severe and as the ambient interference approaches the signal frequencies, second-order rejection becomes necessary.

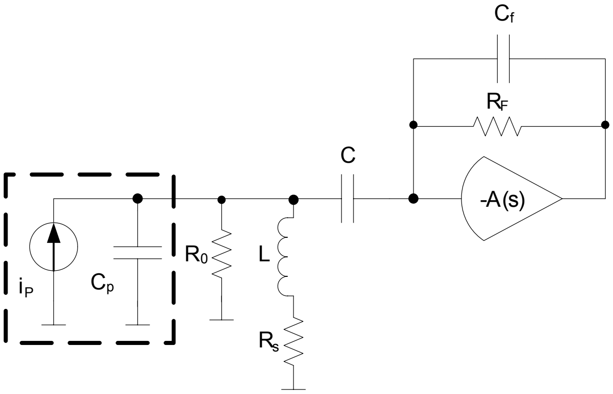

Figure 5: 2nd Order LC Cancellation

The ideal transimpedance gain for the amplifier in Figure 5 is

$$Z(s) = -R_F \frac{\omega_0^2 R_s C s(\tau_s s + 1)}{s^2 + 2\zeta\omega_0 s + (1+\alpha)\omega_0^2} \frac{1}{\tau_f s + 1}, \qquad (5)$$

where $\omega_0^2 = 1/LC$, $\zeta = \frac{1}{2}(\frac{R_s}{Z_0} + \frac{Z_0}{R_0})$, $Z_0 = \sqrt{L/C}$, $\alpha = R_s / R_0$ and $\tau_s = L / R_s$ when $C_p = 0$ and $A(s) = \infty$. $\tau_f = R_f C_f$ is the time-constant of the closed-loop pole from feedback lead compensation.

Loop stability is determined by the loop transmission

$$L(s) = \frac{A(s)\left(s^2 + 2\zeta\omega_0 s + (1+\alpha)\omega_0^2\right)\left(\tau_f s + 1\right)}{\tau_f s^3 + \left(2\zeta\omega_0\tau_f + \frac{R_f}{R_0} + 1\right)s^2 + 2\zeta'\omega_0 s + (1+\alpha)\omega_0^2}, \qquad (6)$$

where $\zeta' = \frac{\omega_0}{2}\left(\tau_f + R_f C\right)\left(1+\alpha\right) + \zeta$.

IV. ACTIVE REJECTION CIRCUITS

A. *Gyrated Transimpedance Amplifier*

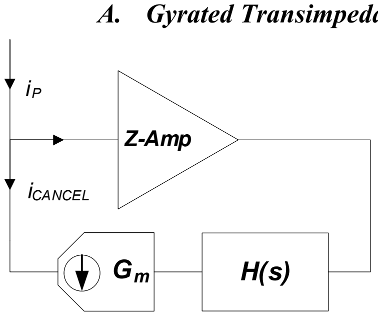

Figure 6: Gyrated Transimpedance Amplifier

Figure 6 shows a transimpedance amplifier with feedback cancellation that gyrates H(s). This is the topology used by Phang and Johns[8] with first order $H(s) = G_0 / 1 + \tau s$ and a single MOS device G_m-generator without source degeneration. The main disadvantage to this topology is that the cancellation loop gain $G_m Z$ is coupled to the signal gain Z. This makes signal gain control such as gain switching or automatic gain control more difficult since it directly affects the cancellation bandwidth.

Higher order cancellation can also be achieved by increasing the order of H(s), albeit with some appropriate compensation.

Because degeneration was not used, the cancellation loop gain and hence rejection bandwidth is strongly dependent on DC photocurrent. As we will see in the next section, resistive degeneration improves both the noise and dynamics.

B. *2nd Order Cancellation with a Tandem Gyrator*

A better strategy would be to use tandem rejection with a gyrator. This reduces the coupling of the cancellation path from the signal path so that there is better separation of the cancellation loop dynamics from the transimpedance amplifier. For example, separate automatic gain control for the signal amplification and for cancellation could then be implemented without the dynamics of one significantly affecting the other.

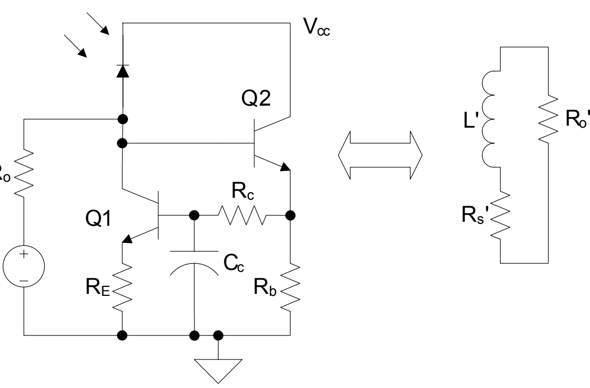

Figure 7: Bipolar implementation of a gyrator circuit and its passive analogue.

The second-order cancellation in Figure 5 can be implemented using the ground-referenced gyrator shown in Figure 7, which is designed for low supply voltage and low noise. The effective inductance is given by

$$L' = \frac{R_{eff} C_c}{G_m}, \qquad (7)$$

where R_{eff} is the resistance seen at the base of Q1, $G_m = g_{m0} /(1 + g_{m0} R_E)$ is the effective transconductance for $\beta \to \infty$ and g_{m0} is the device transconductance of Q1. In Figure 7,

$$R_s' = 1/G_m, \qquad (8)$$

R_o' is the output resistance of Q1 in parallel with R_o. The nominal inductance (at 1mA DC photocurrent) was chosen to be 16 mH and $R_E = 200\Omega$.

Emitter degeneration is used to reduce the variation of G_m with DC photocurrent (Figure 8), hence placing an upper bound on the loop gain of the gyrator and placing a bound on L', thereby reducing the variation in cancellation as well as variation in the op-amp loop transmission. Another key feature of emitter degeneration is the reduction of the current noise contribution of the gyrator. Figure 9 shows that at high collector currents, current noise is dominated R_E, while at low currents by collector shot noise.

The caveat to too much emitter degeneration is that at high DC photocurrent levels, the voltage across the photodiode is reduced. At low supply voltages, this might mean a significant increase in the junction capacitance of the photodiode, and at worst saturation of both Q1 and the photodiode.

In addition to setting ζ in (5), R_o places a lower bound on the transconductance at low DC photocurrents by maintaining a bias current $I_B \approx V_B / R_o$ for $V_B \gg I_P R_E + 2V_{BE}$. Although, R_o contributes current noise $i_n = \sqrt{4kT/R_o}$, for typical values of R_o and I_B, this corresponds to values much smaller than the photodiode shot noise at that same current. One typically designs these circuits such that $R_0 \gg \left| Z_f / A(s) \right|$ over the signal passband so that the signal gain is relatively unaffected.

In Figure 10, one notices that the damping ratio increases as DC photocurrent is decreased. In applications where ringing may be a problem[1], one chooses critical damping, i.e. $\zeta = 1$, at the maximum $G_m = 1/R_E$. From (7) and (8), the low frequency breakpoint τ_s in (5) is invariant to DC photocurrent and is given by the time constant $R_{eff} C_c$.

The reduction of low frequency rejection at low DC photocurrents is apparent in Figure 11. This is so because the shunt impedance Z_{ip} starts to look only resistive so that the rejection reverts to the first-order case shown in Figure 3. The bias current I_B places a lower limit on the DC photocurrent, but also determines the noise floor through the shot noise contribution of the G_m-generator in Figure 9.

The cancellation transfer function $Z(s)$ was chosen so that the step response (Figure 12) is critically damped at the maximum DC photocurrent. In applications where the signal bandwidth is not so wide, such as in FM or FSK (frequency-shift keying), and where a sharper cancellation cut-off is desired, a higher Q and hence lower ζ circuit can be designed.

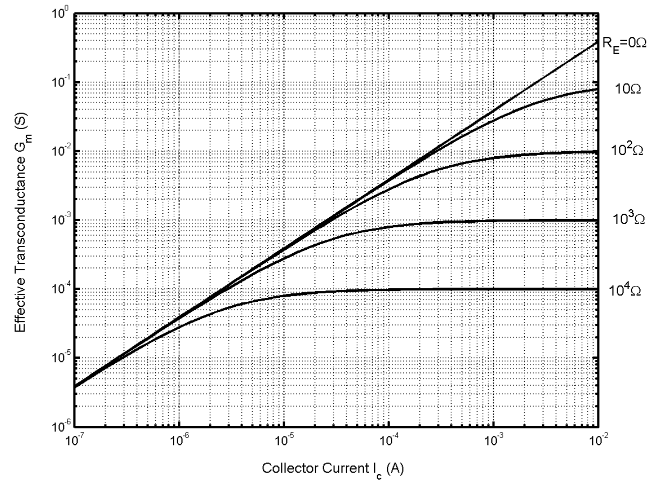

Figure 8: Emitter degeneration R_E reduces the effective transconductance variation in a bipolar device.

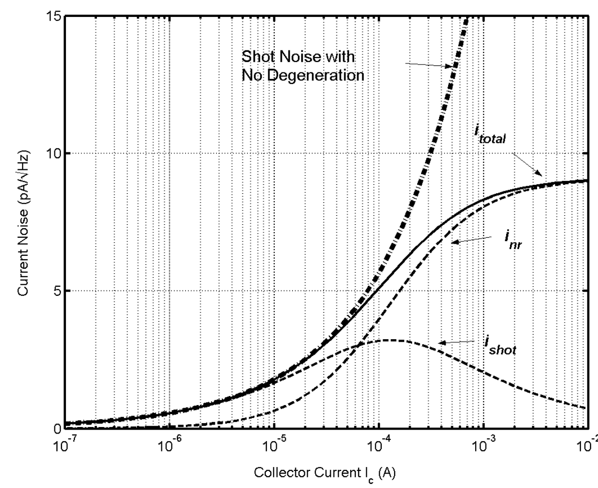

Figure 9: Shot noise contribution at high ambient photocurrents is reduced by emitter degeneration (R_E = 200 Ohms). i_{nr} is the degeneration resistor noise and i_{shot} is the degenerated shot noise.

[1] This is the case in pulse modulation applications such as IrDA.

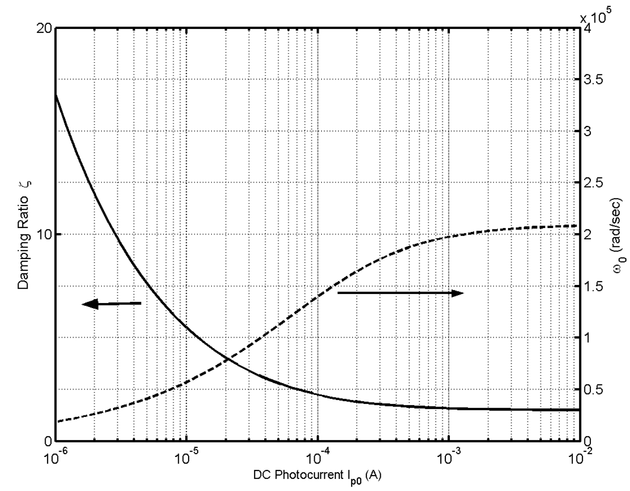

Figure 10: Damping ratio ζ and undamped natural frequency ω_0 of the transimpedance gain Z(s) as DC photocurrent is varied.

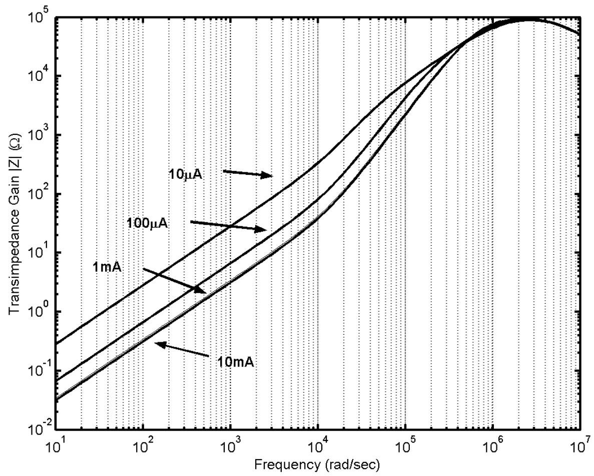

Figure 11 Transimpedance Gain with 2nd Order Rejection at various DC photocurrents. $\zeta \approx 1$ at 1mA.

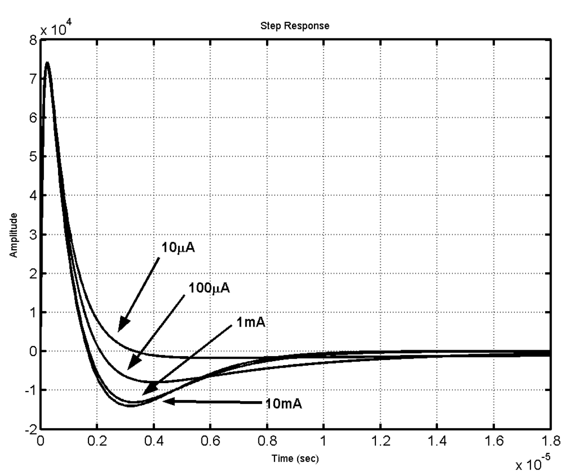

Figure 12: Overall Step Response at various DC photocurrents. $\zeta \approx 1$ at 1mA.

C. Operational Amplifier Stability

The op amp loop transmission $L(s)$ consists of four poles and three zeros. In general, two of the zeros are complex, with locations that are determined by ζ, ω_0 and α in (5), which are dictated by the desired cancellation characteristics in the transimpedance gain $Z(s)$. The root locus plot of the op amp loop transmission in Figure 13 shows that the loop is conditionally stable at high DC photocurrents because the lightly damped complex pole pair traverses the imaginary axis into the right-half plane at small loop gains. Therefore, saturation of the op amp output should be avoided. At lower photocurrents, the poles are better damped. Otherwise, Figure 14 shows that the loop has good phase and gain margins.

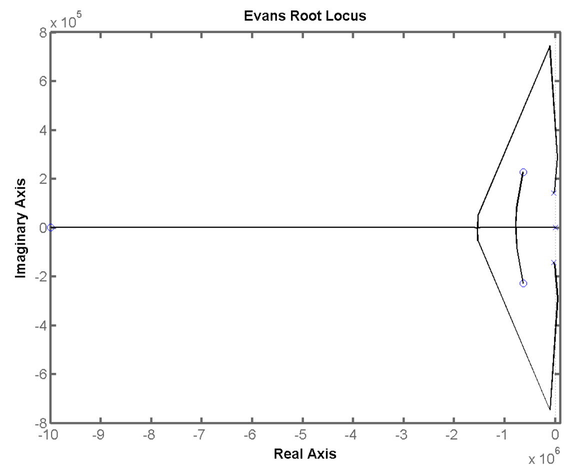

Figure 13: Evans Root Locus plot of L(s) for $\zeta \approx 1$ and DC photocurrent of 10 mA. The high frequency pole from the lead compensator is not shown.

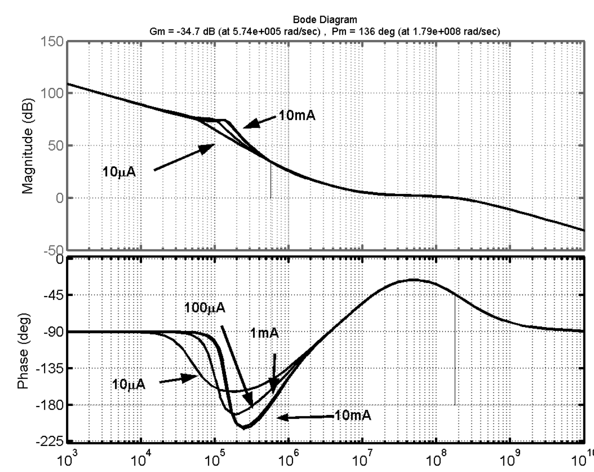

Figure 14: Bode Plots of the Op-Amp Loop Transmissions L(s) at various DC photocurrents. $\zeta \approx 1$ at 1mA.

D. Effect of Parasitic Junction Capacitance C_p

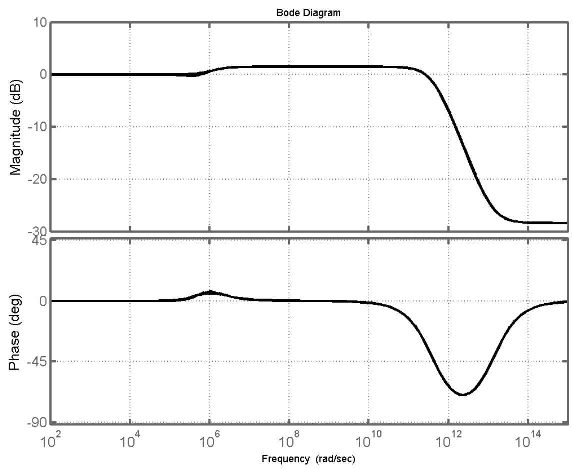

Figure 15: Bode Plot of $U_p(s)$ shows the added gain and phase to the loop transmission due to C_p. DC Photocurrent from 10μA to 10 mA. C_p=0.15*C*.

Using Middlebrook's Extra Element Theorem [10], the effect of junction capacitance C_p on the loop transmission is given by

$$U_p(s) = \frac{1 + C_p s (Z_1 \| Z_2)}{1 + C_p s \left[Z_1 \| (Z_2 + Z_3) \right]} \qquad (9)$$

where $Z_1 = (Ls + R_s) \| R_o$, $Z_2 = 1/Cs$, $Z_3 = R_f \| 1/C_f s$ and the new loop transmission is given by $L'(s) = L(s)U_p(s)$.

Figure 15 shows C_p contributes very little to the dynamics at or below crossover of the op amp feedback loop when $C_p \ll C$. The "bump" at 10^6 rad/sec is well below the crossover of the op amp feedback loop and corresponds to a variation of only about 1.5 dB in magnitude and 6.5 degrees in phase.

E. Stability of the Cancellation Loop

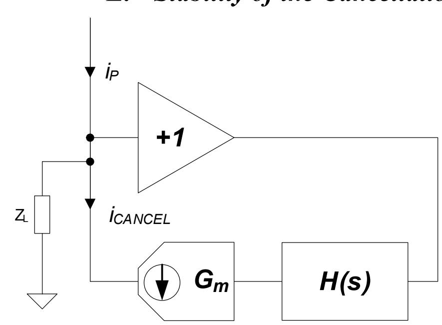

Figure 16: Cancellation Loop

The cancellation loop shown in Figure 16 is a gyrator loaded by an impedance Z_L. Z_L consists of the R_o, C_p, C and Z_{dp}, the driving point impedance at the input of the transimpedance amplifier in Figure 5,

$$Z_L = R_0 \| \frac{1}{C_p s} \| \left(\frac{1}{Cs} + Z_{dp} \right). \qquad (10)$$

The loop transmission of the loaded gyrator is then

$$L(s) = G_m Z_L H(s). \qquad (11)$$

The driving point impedance Z_{dp} has a high pass characteristic and looks inductive at low frequencies with an inductance that is $L_{dp} = R_f / A_0$,

$$Z_{dp} = \frac{\frac{R_f}{A_0} s}{(1 + R_f C_f s)(s / A_0 + 1)}. \qquad (12)$$

To a reasonable approximation, if $\omega_{dp} = 1/\sqrt{L_{dp} C}$, $1/R_f C_f$ and A_0 occur well above the cancellation loop crossover, Z_{dp} can be ignored. This simplification allows us to lump C_p with C to create a pole with R_o. The cancellation loop transmission is shown in Figure 17. In fact, it can be shown that the phase margin of this loop is directly related to ζ in (5) [11].

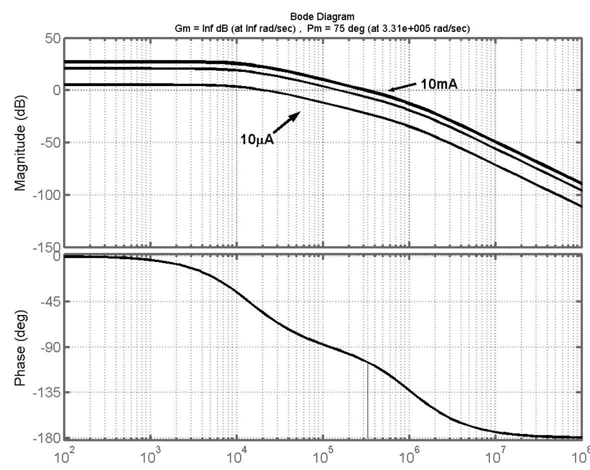

Figure 17: Bode plot of the gyrator loop transmission at various DC photocurrents. $\zeta \approx 1$ at 1mA.

F. Results

The measured step response shown in Figure 18 agrees well with theory and simulation (Figure 12). The circuit performs well when receiving IrDA data, which consists of narrow pulses, as shown in Figure 19. The data was received from an IrDA beacon for outdoor applications. The system is designed to receive data in direct sunlight.

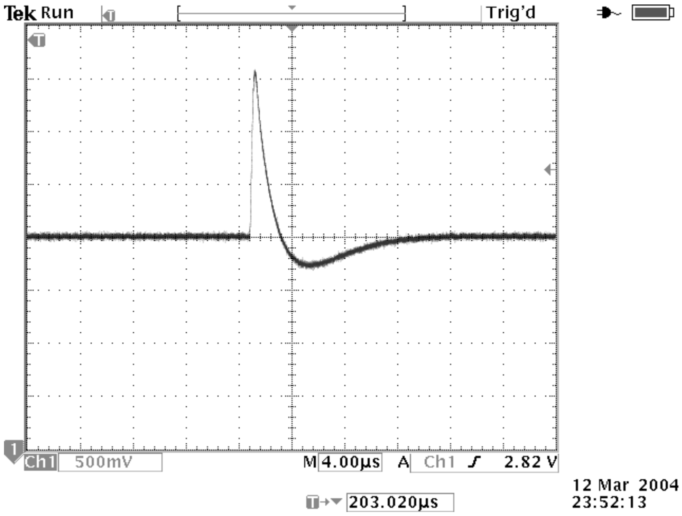

Figure 18: Measured step response with 375µA of DC photocurrent.

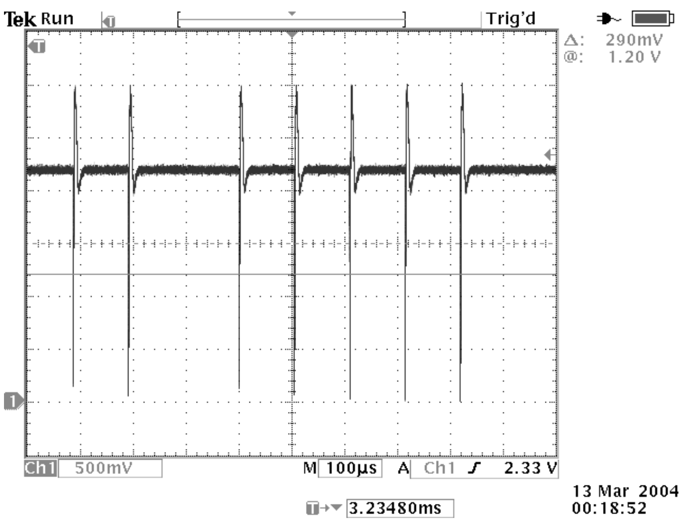

Figure 19: IrDA Byte with 275µA of DC photocurrent.

V. CONCLUSIONS

We have analyzed some of the key issues in the design of ambient photocurrent rejection circuits, and have presented and demonstrated a circuit design that avoids explicit automatic gain control to cancel the effect of varying DC photocurrent. Automatic gain control typically introduces additional dynamics, increases noise and adds complexity.

Passive analogues are used as models to analyze active rejection circuits. This yields design intuition and insight into stability, transient response, rejection performance and noise. Measurements confirm the theory and simulations, and performance in an IrDA application was demonstrated.

VI. REFERENCES

[1] E. C. Lupton, S. B. Leeb, G. B. Hovorka, D. Jackson, and B. L. Bentzen, "Communication System." US Patent 6,400,482: Talking Lights, LLC, 2002.

[2] D. T. Burke, S. Leeb, R. T. Hinman, E. C. Lupton, J. Burke, J. C. Schneider, B. Ahangar, K. Simpson, and E. A. K. Mayer, "Using talking lights to assist brain-injured patients with daily inpatient therapeutic schedule," *Journal of Head Trauma Rehabilitation*, vol. 16, pp. 284-291, 2001.

[3] R. T. Hinman, E. C. Lupton, S. B. Leeb, A. T. Avestruz, R. Gilmore, D. Paul, and N. Peterson, "Using talking lights illumination-based communication networks to enhance word comprehension by people who are deaf or hard of hearing," *American journal of audiology*, vol. 12, pp. 17-22, 2003.

[4] G. Livshin, A.-T. Avestruz, R. T. Hinman, E. C. Lupton, and S. B. Leeb, "Context Aware Security Based on Illumination (CASI)," presented at IEEE Conference for Technologies for Homeland Security Conference, Cambridge, MA, 2003.

[5] A.-T. Avestruz, E. C. Lupton, R. T. Hinman, and S. B. Leeb, "Smart Markers for In-Depth Battlefield Information: Optical and Hybrid Communication," presented at 2002 Army Science Conference, Tampa, FL, 2002.

[6] A. J. C. Moreira, R. T. Valadas, and A. M. de Oliveira Duarte, "Characterisation and modelling of artificial light interference in optical wireless communication systems," presented at Personal, Indoor and Mobile Radio Communications, 1995. PIMRC'95. 'Wireless: Merging onto the Information Superhighway'., Sixth IEEE International Symposium on, 1995.

[7] G. Yun and M. Kavehrad, "Spot-diffusing and fly-eye receivers for indoor infrared wireless communications," presented at Wireless Communications, 1992. Conference Proceedings., 1992 IEEE International Conference on Selected Topics in, 1992.

[8] K. Phang and D. A. Johns, "A CMOS optical preamplifier for wireless infrared communications," *Circuits and Systems II: Analog and Digital Signal Processing, IEEE Transactions on [see also Circuits and Systems II: Express Briefs, IEEE Transactions on]*, vol. 46, pp. 852-859, 1999.

[9] J. G. Graeme, *Photodiode Amplifiers: Op Amp Solutions*, First ed. New York: McGraw-Hill, 1995.

[10] R. D. Middlebrook, "Null Double Injection and the Extra Element Theorem," *IEEE Transactions on Education*, vol. 32, pp. 167-180, 1989.

[11] J. K. Roberge, *Operational Amplifiers: Theory and Practice*. New York: John Wiley and Sons, 1975.